



Technical note: Novel analytical solution for groundwater response to atmospheric tides

Jose M. Bastias Espejo¹, Chris Turnadge², Russell S. Crosbie², Philipp Blum¹, and Gabriel C. Rau³

¹Institute of Applied Geosciences (AGW), Karlsruhe Institute of Technology, Karlsruhe (KIT), Germany

²CSIRO Land and Water, Adelaide, Australia

³School of Environmental and Life Sciences, The University of Newcastle, Callaghan, Australia

Correspondence: Jose M. Bastias Espejo (jose.bastias@kit.edu)

Abstract.

Subsurface hydraulic and geomechanical properties can be estimated from well water level responses to Earth and atmospheric tides. However, the limited availability of analytical solutions restricts the applicability of this approach to realistic field conditions. We present a new and rigorous analytical solution for modelling flow between a subsurface-well system caused by harmonic atmospheric loading. We integrate this into a comprehensive workflow that also estimates subsurface properties using a well-established Earth tide method. When applied to groundwater monitoring datasets obtained from two boreholes screened in a sand aquifer in the Mary-Wildman Rivers region (Northern Territory, Australia), estimated hydraulic conductivity and specific storage agree. Results also indicate that small vertical leakage occurs in the vicinity of both boreholes. Furthermore, the estimated geomechanical properties were within the values reported in literature for similar lithological settings. Our new solution extends the capabilities of existing approaches, and our results demonstrate that analysing the groundwater response to natural tidal forces is a low-cost and readily available solution for unconsolidated, hydraulically confined, and undrained subsurface conditions. This approach can support well-established characterisation methods, increasing the amount of subsurface information.

1 Introduction

Knowledge of subsurface hydro-geomechanical properties is crucial for Earth resource development and management. Such properties determine the capacity of hydrostratigraphic units to store and transmit groundwater. Traditional, active hydraulic testing methods such as pumping, slug, pressure and packer tests or laboratory analyses of cores involve considerable logistical expenses (Maliva, 2016). In contrast, passive methods (e.g. *Tidal Subsurface Analysis*, TSA), which are used to estimate hydraulic properties from well water level responses to ubiquitous periodic forces (Merritt, 2004; Cutillo and Bredehoeft, 2011), are relatively low cost to implement and derive additional value from commonly measured datasets (McMillan et al., 2019; Rau et al., 2020, 2022). The effect of gravitational effects and atmospheric loading on the subsurface has been long observed and reported (Meinzer, 1939) and is contained in routine groundwater pressure measurements made in countless observation wells around the world (McMillan et al., 2019). The influence of natural forces such as tides on groundwater pressures are ubiquitous allowing widespread application reducing effort and cost of investigations. Since passive approaches



25 rely on natural signals and do not require any active perturbation of the subsurface system, we will refer to them collectively
as *Passive Subsurface Characterisation* (PSC) in our work.

Earth and atmospheric tides act as harmonic forces at various frequencies (McMillan et al., 2019). For groundwater
investigation the most informative frequencies range from 0.8 to 2.0 cycles per day (cpd) (Merritt, 2004). Dominant frequencies
present in groundwater pressure measurements are the S_1 (1.0 cpd), M_2 (1.93 cpd) and the S_2 (2.00 cpd). These components
30 generally show a higher amplitude in comparison with other tidal harmonics and are, therefore, more likely to be contained in
field datasets (McMillan et al., 2019).

Loading forces cause mechanical deformation of the water-saturated porous medium, leading to an instantaneous pore
pressure response and a hydraulic gradient towards the nearby observation well. This gradient drives groundwater exchange
between the subsurface and the well until re-equilibrium is achieved (Cheng, 2016; Verruijt, 2013; Wang, 2017). The am-
35 plitude ratio between the magnitude of well water level variation and subsurface pore pressure variation, as well as the time
delay required for groundwater exchange, expressed as a phase shift or phase lag, can be used to estimate subsurface hydro-
geomechanical properties (Hsieh et al., 1987). Positive phase shifts (i.e., when well water levels respond before subsurface wa-
ter pressures to Earth tide-induced strain variations) have been linked to vertical connectivity with adjoining hydrostratigraphic
units (Roeloffs et al., 1989). Amplitude ratios and phase shifts can be readily extracted from measurements and inverted using
40 established analytical solutions (McMillan et al., 2019).

Cooper Jr et al. (1965) derived an analytical solution for the movement of groundwater caused by seismic waves in fully
confined aquifers. Bredehoeft (1967) proposed a method to interpret the effect of Earth tides on observation wells based on
classic solid mechanics, which allowed the estimation of specific storage of the aquifer if the Poisson's ratio of the porous
medium was known. However, this method did not comply with Biot consolidation theory (Biot, 1941) as it did not couple
45 fluid dynamics with mechanical deformation. Subsequently, many studies described the effect of Earth tides in poroelastic
systems (Bodvarsson, 1970; Robinson and Bell, 1971; Arditty et al., 1978; Van der Kamp and Gale, 1983), but did not consider
the damping effect of the observation well on the amplitude and phase. To address the signal diminishing effect of a well,
Hsieh et al. (1987) combined the poroelastic response of a confined aquifer with Cooper Jr et al. (1965)'s work and derived an
analytical solution to model flow to wells due to Earth tides.

50 Rojstaczer (1988) proposed an analytical solution for modelling flow to wells induced by atmospheric tides. However, the
solution requires knowledge of vadose properties which are often unknown, and it does not account for the effect of barometric
efficiency on confined pore pressure (also known as tidal efficiency). To address this, Rojstaczer and Riley (1990) developed
an analytical solution that includes the barometric effects on confined pore pressure, but it does not consider the effects on
amplitude and phase shift of a well. Additionally, the mean stress in their formulation only considers the vertical direction and
55 neglects lateral directions, which can lead to significant errors for typical Poisson's ratio values (Cheng, 2016; Verruijt, 2013;
Wang, 2017).

Several studies have estimated subsurface properties using Earth tide analysis (Le Borgne et al., 2004; Doan et al., 2006;
Cutillo and Bredehoeft, 2011; Lai et al., 2013, 2014; Rahi and Halihan, 2013; Xue et al., 2016; Shi and Wang, 2016; Acworth
et al., 2016). However, many of the analytical solutions used to derive estimates assume oversimplified settings, which can



60 lead to inaccurate results. To address this, Wang et al. (2018) recently developed an analytical solution that describes flow in
and out of a well caused by Earth tides in a two-layered flow system. Gao et al. (2020) accounted for the well skin effect,
which occurs when the physical properties of the formation in a larger area around a borehole are affected by drilling, leading
to reduced amplitude ratio and phase shift. Additionally, Guo et al. (2021) derived an analytical solution to describe flow in
fractures caused by Earth tides and estimated hydraulic properties. Finally, Liang et al. (2022) solved Richards equation (Freeze
65 and Cherry, 1979) to include the effect of the unsaturated zone, finding that it delays the phase shift response of the borehole
pressure.

Xue et al. (2016) and Rau et al. (2020) used the analytical solution of Wang (2017) to model the barometric effect of
atmospheric tides with vertical leakage, but it lacks the damping effect of an observation well. Recently, Rau et al. (2022)
proposed a new approach based on the work of Acworth et al. (2017) that combines poroelastic relations for one-dimensional
70 Earth and atmospheric tide deformation to obtain a system of equations with poroelastic properties. However, their approach
is based on an analytical model that does not correctly represent vertical leakage. To the best of our knowledge, there is no
rigorous analytical solution in the literature to model flow to wells induced harmonically from atmospheric tides based on the
mean stress flow equation while considering a semi-confined aquifer.

The objective of this work is twofold. Firstly, we introduce a new analytical solution based on the Biot theory of consolidation
75 that describes the flow between a subsurface-well system caused by the harmonic loading of atmospheric tides. Secondly, we
demonstrate its usefulness by applying it to well water levels from two boreholes in the Northern Territory of Australia and
comparing the results with established Earth tide methods and existing knowledge of the groundwater system. Our study
demonstrates that our new analytical solution extends the range of properties that can be accurately estimated and provides a
better understanding of subsurface processes and properties.

80 2 Analytical solution

In this section, a new analytical solution based on the mean stress flow equation is derived to simulate flow to wells resulting
from atmospheric tides loading the surface. The fluid continuity equation in the mean stress form can be used to describe the
water flow from a semi confined aquifer towards an observation well. If only radial flow is assumed and small vertical fluid
exchange from the semi confined layer occurs, the equation reads (Cheng, 2016; Verruijt, 2013; Wang, 2017)

$$85 \quad S_{\sigma} H_a \left(\frac{\partial h}{\partial t} - \frac{\alpha}{3K S_{\sigma}} \frac{\partial \sigma}{\partial t} \right) = T \left[\frac{\partial^2 h}{\partial r^2} + \frac{1}{r} \frac{\partial h}{\partial r} \right] - \frac{k_l}{H_l} h. \quad (1)$$

Here, σ is the mean stress; K is the drained bulk modulus of the solid material; r radius; hydraulic head of the fluid (groundwater for this study), h is being used as a proxy for pore pressure $p_f = \rho g h$; T is the transmissivity of the aquifer with $T = k_a H_a$,
where k_a is the hydraulic conductivity and H_a the aquifer thickness. If the aquifer is overlain by a leaky aquitard, then the
downward leakage flux can be described as $k_l h H_l^{-1}$, where k_l is the vertical hydraulic conductivity and H_l is the aquitard
90 saturated thickness. Note that this approximation is only valid when $k_a k_l^{-1} \gg 1$. α is the Biot coefficient which is equal to
one for unconsolidated systems (e.g., gravels, sands and clays), and ranges between $n \leq \alpha \leq 1$ for consolidated systems (e.g.



bedrock); where n is effective porosity. S_σ is the Biot modulus at constant stress (also known as three dimensional storage coefficient) (Cheng, 2016; Verruijt, 2013; Wang, 2017)

$$S_\sigma = \frac{\rho g}{R}, \quad (2)$$

95 where g is gravitational acceleration and ρ the fluid density. R is the Biot modulus at constant stress defined as (Cheng, 2016; Verruijt, 2013; Wang, 2017)

$$\frac{1}{R} = \frac{n}{K_f} + \frac{\alpha - n(1 - \alpha)}{K}, \quad (3)$$

where K_f is the bulk modulus of the fluid ($K_f = 2.2 \cdot 10^9$ Pa for freshwater).

100 Barometric pressure fluctuations cause loading at the ground surface which results in vertical deformation of the subsurface and, therefore, changes to the internal stress balance of the fluid-solid skeleton system. For example, when atmospheric pressure rises and, the formation undergoes compressive stress resulting in an increased in the confined pore pressure (Domenico and Schwartz, 1997).

In a fully saturated porous medium, this effect can be described by Biot consolidation theory as follows (Cheng, 2016; Verruijt, 2013; Wang, 2017)

105
$$p_f = R \left(-\frac{\alpha}{K} \sigma + \xi \right). \quad (4)$$

Here, p_f is the fluid (i.e., water in this study) pore pressure; σ is the mean stress; K is the drained bulk modulus of the solid material; ξ is the change in fluid content, can be used to quantify changes in pore pressure resulting from hydraulic gradients (Cheng, 2016; Verruijt, 2013; Wang, 2017). The sign of this parameter indicates whether a fluid is leaving or entering a given porous medium.

110 Biot's consolidation theory assumes $\xi = 0$ when undrained conditions apply within the porous medium. Conversely, system conditions are drained when $\xi \neq 0$. Note here that a drained porous medium conceptually differs from a confined aquifer and these concepts that are often mixed up in the literature. For example, a confined aquifer may exchange fluid via one of its horizontal boundaries such as a confined aquifer bounded by a river.

115 We solved Eq. 1 for steady state conditions to obtain the periodic water level in an open borehole $h_w^{AT} = h_{w,o}^{AT} e^{i\omega t}$ due to atmospheric loading, where ω is the angular frequency of the tide signal and superscript AT stands for atmospheric tides, for example S_1 at 1 cycle per day (CPD) or the atmospheric response to S_2 at 2 cpd (Merritt, 2004; McMillan et al., 2019).

As boundary condition, the hydraulic head far away from the radius of influence of the borehole is given only by the mechanical response of the system

$$t > 0, r = r_\infty : h(r, t) = h_\infty = \frac{p_{f,\infty}}{\rho g}, \quad (5)$$

120 where r_∞ is a distance far away from the radius of influence of the borehole and the hydraulic head at the borehole screen, h_w , should be the water level in the bore

$$t > 0, r = r_w : h(r, t) = h_w^{AT}(t), \quad (6)$$



the bore and the aquifer are free to exchange groundwater, i.e.,

$$t > 0, r = r_w : 2\pi r_w T (\partial h / \partial r) = \pi r_c^2 (\partial h_w^{AT} / \partial t). \quad (7)$$

125 With these boundary conditions the solution of the water level in the borehole is derived as

$$h_{w,o}^{AT} = \frac{i\omega H_a}{(i\omega(S_\epsilon + \frac{\rho g}{K})H_a + k_l/H_l)\gamma_a} \left(\frac{\sigma}{3K} \right), \quad (8)$$

where the periodic atmospheric loading is assumed only vertical (i.e. $\sigma = \sigma_{zz}$) modelled as $\sigma = \sigma_{atm} e^{i\omega t}$, thus σ_{atm} represents the amplitude of the atmospheric tide, and

$$\gamma = 1 + \left(\frac{r_c}{r_w} \right)^2 \frac{i\omega r_w K_0(\beta r_w)}{2T\beta K_1(\beta r_w)}. \quad (9)$$

130 Here, K_0 and K_1 are the modified Bessel functions of the second kind and order zero and one, respectively, and

$$\beta = \left(\frac{k_l}{TH_l} + \frac{i\omega(S_\epsilon + \frac{\rho g}{K})H_a}{T} \right)^{0.5}. \quad (10)$$

Note that S_ϵ , the specific storage at constant strain, and S_σ are related as (Cheng, 2016; Verruijt, 2013; Wang, 2017)

$$S_\epsilon = S_\sigma - \frac{\rho g}{K}. \quad (11)$$

135 Since it is assumed that the borehole is open to the atmosphere, any change in barometric pressure will also play a role in the hydrostatic pressure inside the borehole. Thus, the amplitude ratio between the atmospheric loading and the confined pore pressure due to atmospheric tides, A^{AT} , has to be expressed as the balance between the far field pore pressure ($p_{f,\infty}(\rho g)^{-1}$, Eq. 4), the amplitude of the atmospheric load ($\sigma_{atm}(\rho g)^{-1}$) and the change of fluid level in the well, $h_{w,o}$, such as

$$A^{AT} = \left| \frac{p_{f,\infty} - \sigma_{atm} - (\rho g)h_{w,o}^{AT}}{\sigma_{atm}} \right|. \quad (12)$$

The time lag between the far field confined pore pressure and the actual change of fluid in an open well is given by

$$140 \Delta\phi^{AT} = \arg \left(\frac{p_{f,\infty} - \sigma_{atm} - (\rho g)h_{w,o}^{AT}}{\sigma_{atm}} \right). \quad (13)$$

Note that the applied amplitude of the periodic stress at a boundary has to be equal to the atmospheric pressure

$$\sigma_{atm} = -P_{atm}, \quad (14)$$

where P_{atm} is the barometric pressure measured in the field. In this convention, the compression stress is opposite in sign compared to the atmospheric pressure as an increase compresses the subsurface.

145 We have named our novel analytical solution as the *mean stress solution*. Drawing an analogy to the established Earth tide methods (Hsieh et al., 1987; Wang et al., 2018, e.g.), our new solution enables the estimation of subsurface hydraulic and geomechanical properties from atmospheric tidal components that are ubiquitous in standard field measurements of well water levels. This innovative solution expands the scope of existing approaches that passively characterise subsurface processes and properties (McMillan et al., 2019).



150 3 Field application

3.1 Field site and groundwater monitoring

In this section, we apply our analytical solution to field data, compare the results with those derived from established Earth tide methods and consider the results in the context of existing knowledge such as from lithological logs and hydraulic testing. The overall workflow applied in this section is shown in Fig. 1 which incorporates established Earth tide methods alongside
155 our new solution.

The study area is bounded by the Mary River National Park in the west and by the Kakadu National Park in the east. The intervening area has been of interest for irrigated agricultural development since the 1980s. The area features a sub-equatorial climate, with the dry season occurring between May and September and the wet season occurring between October and April. The highest annual mean air temperatures are recorded between October and December at around 35°C and the lowest in July
160 at around 16°C (Tickell, 2017).

Two main hydrostratigraphic units are present as layers in the study area: (1) Mesozoic/Cenozoic sediments underlain by (2) the Proterozoic Koolpinyah Dolostone, and silt- and sandstones (Fig. 2a) (Tickell, 2017). Groundwater and mineral exploration wells are the main source of geological information as outcrops are rare. Mesozoic/Cenozoic sediments consist of unconsolidated to poorly consolidated sands, clayey sands, and clays. Lithological logs indicate that this unit is laterally extensive across
165 the study area (Tickell, 2017). A leaky sandy clay aquitard partially confines a second semi-confined sand aquifer (B1 and B2 in Fig. 2c). This aquifer is sufficiently permeable to allow recharge to the semi-confined sand aquifer, as observed by increases in the groundwater level during each wet season. The Proterozoic strata consist primarily of Koolpinyah Dolostone and Wildman Siltstone. The hydrological behaviour of this unit is conceptually a fractured aquifer (Tickell, 2017). Constant rate discharge pumping tests indicate that the hydraulic conductivity of the Mesozoic/Cenozoic strata ranges from $8.0 \cdot 10^{-5}$ to $6.3 \cdot 10^{-4}$
170 $\text{m}\cdot\text{s}^{-1}$ (Appendix B).

Groundwater monitoring datasets from two boreholes B1 and B2 were analysed in this work (Fig. 2b and Table 1). Note that the original nomenclature from the Australian Northern Territory (NT) was modified (Table 1). The lithological logs indicate that the boreholes are screened in the upper strata (Fig. 2c). In general, the upper two thirds of the profile are clays and sandy clays that confines the underlying aquifer. The lower third often consists of sands, clayey sands and gravels. Sands are mostly
175 present as fine-grained quartz with limited occurrences of coarse sands to pebbles.

Well water levels were monitored hourly between June 2016 and September 2019 in each borehole using InSitu Level TROLL 400 data loggers (InSitu Inc., USA). The measured pressure heads were converted to hydraulic head values by referencing the dips of depth to water level manually to the surveyed top of casing elevations. Concurrently, barometric pressure was recorded from September 2016 to October 2017 using an InSitu BaroTROLL 500 data logger (InSitu Inc., USA).

180 3.2 Extraction of tidal responses

Earth tide strains, barometric pressure and hydraulic heads in wells B1 and B2, are shown in Fig. 3. Outliers were identified using Pearson's rule, i.e., values that deviate more than three times the *Median Absolute Deviation* (MAD) (Pham-Gia and

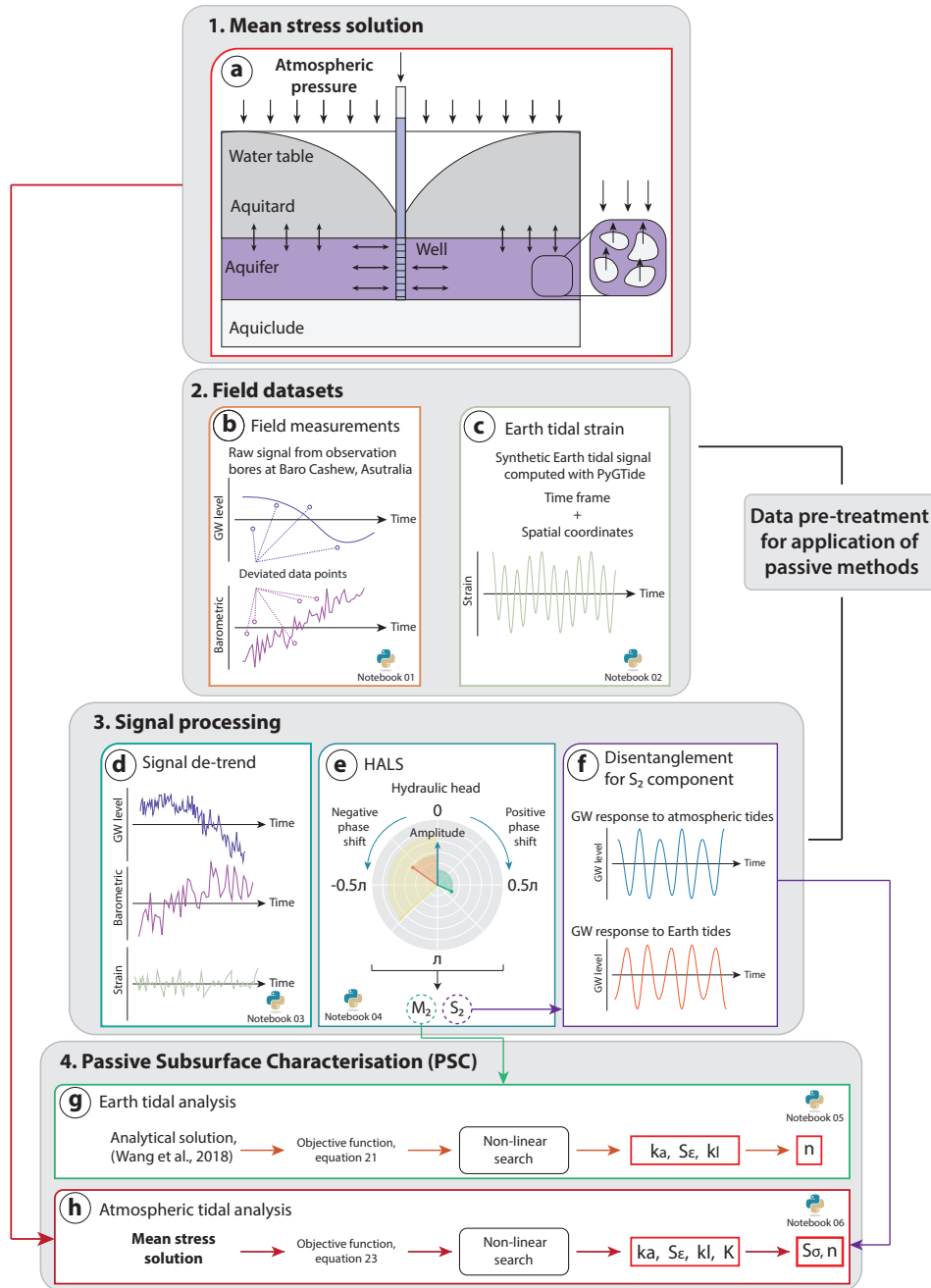


Figure 1. Overview of the workflow applied to estimate subsurface hydraulic and geomechanical properties using the groundwater response to Earth and atmospheric tides. The data set and Python scripts developed for this work are available in an external repository (see Code and Data Availability statements).



Table 1. Groundwater well construction information, reference datum Geocentric Datum Of Australia (GDA) 1994. DD stands for *decimal degrees*.

Borehole NT ID	Borehole	Latitude [DD]	Longitude [DD]	Total depth [m]	Screen length [m]	Radius [m]
RN039769	B1	-12.6077	131.8295	43.0	4	0.156
RN024762	B2	-12.6259	131.8801	61.1	6	0.203

Hung, 2001), and removed from the data (Fig. 1b and A1). Note that the overall head varies by about 2 m reflecting the wet and dry seasons that are typical for tropical Australia. Earth tide strains were calculated using *PyGTide* (Rau, 2018) which is based on the widely used ETERNA PREDICT software Wenzel (1996) (Fig. 1c).

Harmonic tidal components of the ten dominant target frequencies between 0.33 and 2.2 cycles per day (cpd) (Merritt, 2004; McMillan et al., 2019) were extracted from all time series and locations following the methods outlined in Schweizer et al. (2021) and Rau et al. (2020):

- The measured well water levels were de-trended using a moving linear regression filter with a 3-day window (Fig. 1d) and the results are shown in Fig. A2.
- Amplitudes and phases of ten tidal harmonic constituents were jointly estimated using *Harmonic Least Squares* (HALS) (Fig. 1e).
- From HALS, amplitudes and phases of the M_2 and S_2 tidal components were obtained for the Earth tide strains (Fig. 4a), barometric pressure (Fig. 4b) and hydraulic heads (Fig. 4c,d).
- Complete disentanglement of the groundwater response to Earth and atmospheric tide influences was done for S_2 following the method established by Rau et al. (2020) (Fig. 1f).

The resulting amplitude of the hydraulic head (abbreviated as GW for groundwater) A^{GW} can be divided by the Earth tide strain amplitude (abbreviated as ETP for Earth tides) A^{ETP} , to obtain the amplitude ratio (Fig. 4e)

$$A_o^{ET} = \frac{A^{GW}}{A^{ETP}}. \quad (15)$$

The phase shift $\Delta\phi_o^{ET}$, can be obtained as the difference between the obtained phase of the hydraulic head measurements ϕ^{GW} and the computed Earth tide strain prediction, ϕ^{ETP} as

$$\Delta\phi_o^{ET} = \phi^{GW} - \phi^{ETP}. \quad (16)$$

Resulting A_o^{ET} and $\Delta\phi_o^{ET}$ for hydraulic head and areal Earth tide strain for borehole B1 and B2 are presented in Fig. 4e and Table A1.

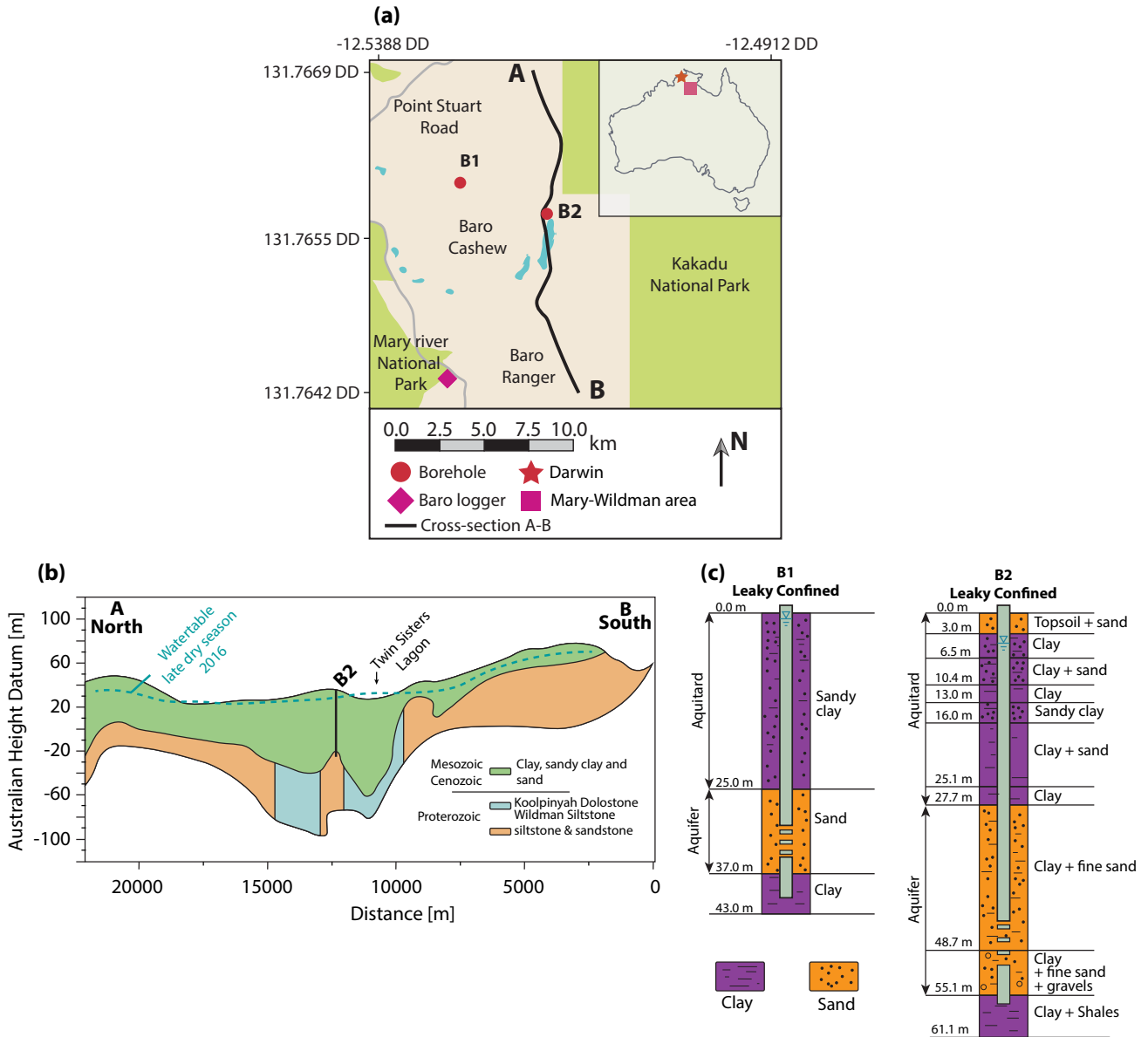


Figure 2. (a) Map of the study site, including surface water features, borehole locations and, location of the transect from A-B, (b) transect showing simplified geology adapted from (Tickell, 2017) and (c) lithological logs from both studied boreholes. *DD* stands for decimal degrees.

205 Analogously, the ratio between the resulting amplitude of HALS of the hydraulic head A^{GW} can be divided by the measured (time series) barometric pressure (abbreviated as *ATP* for atmospheric tides) A_{ATP} to obtain the amplitude ratio

$$A_o^{AT} = \frac{A^{GW}}{A_{ATP}} \rho g. \quad (17)$$

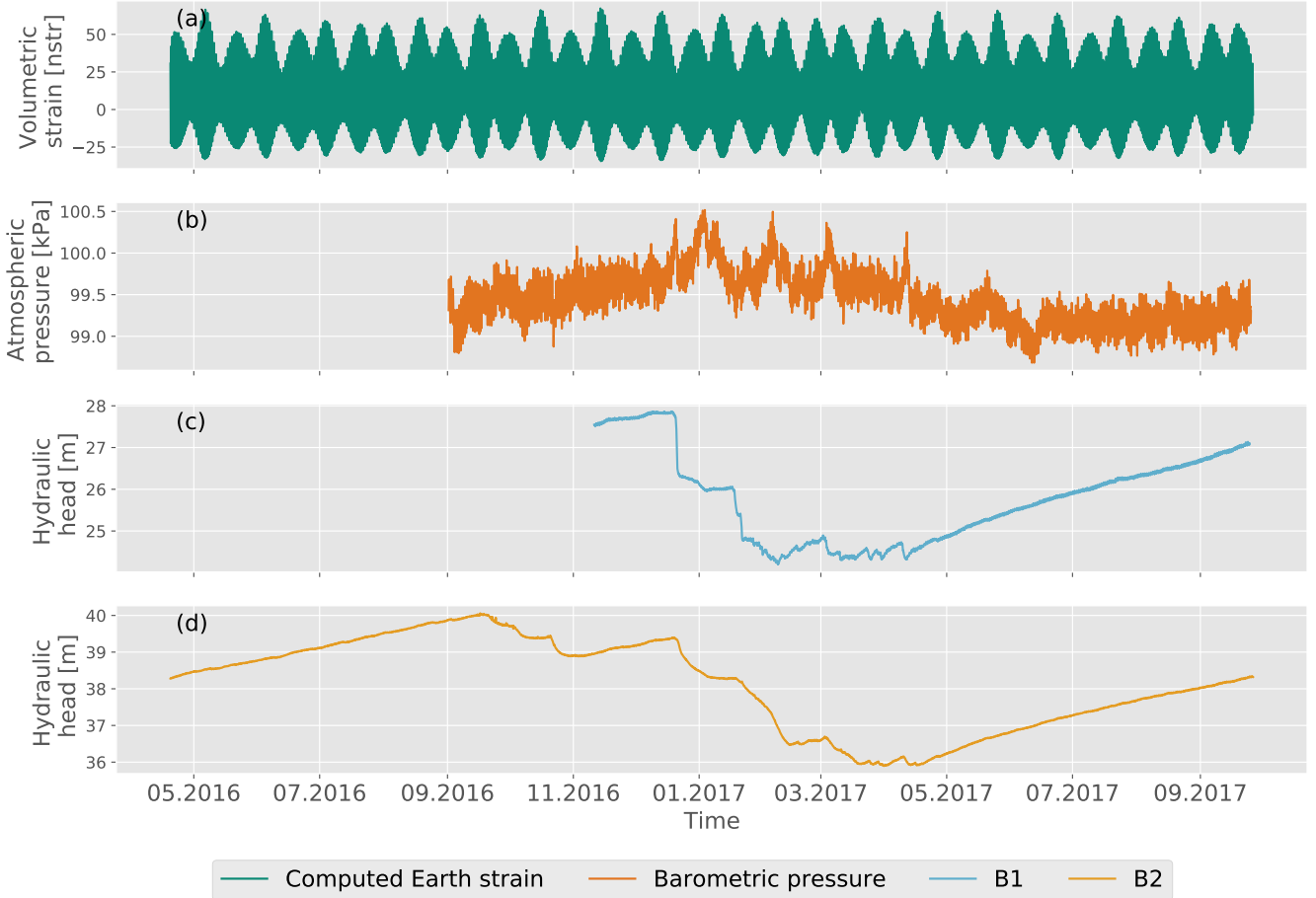


Figure 3. Time series of: (a) computed Earth tide strain in nano-strain (nstr), (b) measurements of barometric pressure, and hydraulic head time series measured in boreholes B1 (c) and B2 (d).

The phase shift $\Delta\phi_o^{AT}$, can be obtained as the difference between the obtained phase of the hydraulic head measurements ϕ^{GW} and the measured barometric pressure, ϕ^{ATP} as

$$210 \quad \Delta\phi_o^{AT} = \phi^{GW} - \phi^{ATP}. \quad (18)$$

Resulting A_o^{AT} and $\Delta\phi_o^{AT}$ for hydraulic head and areal Earth tide strain for borehole B1 and B2 are presented in Fig. 4f and Table A2.

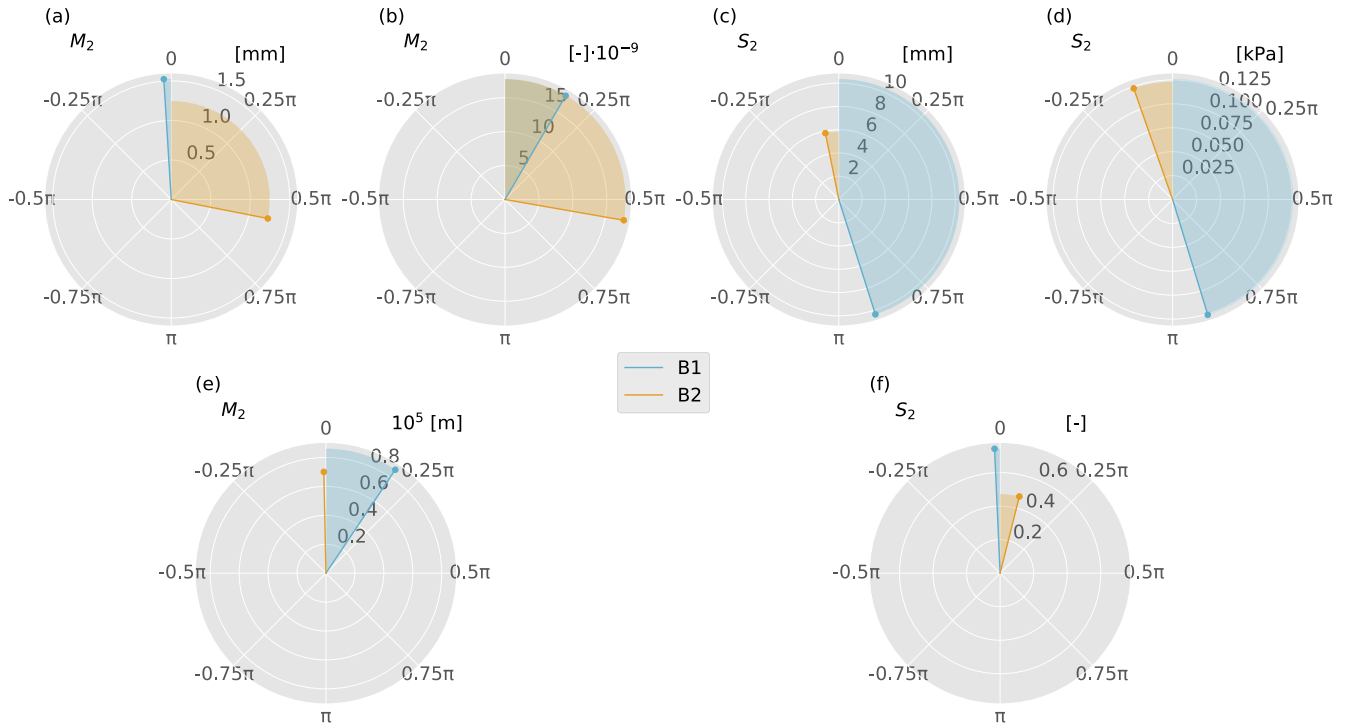


Figure 4. Polar plots showing the M_2 and S_2 harmonics estimated from hydraulic heads in response to Earth and atmospheric tides for boreholes B1 and B2. (a) M_2 constituent in measured well water levels. (b) M_2 constituent in Earth tide strain data calculated at well locations. (c) S_2 constituent in well water levels. (d) S_2 constituent in Earth tide strain data calculated at well locations. (e) Amplitude and phase shift of the M_2 constituent, equations 15 and 16. (f) Amplitude ratio and phase shift of the S_2 constituent, equations 17 and 18 .

3.3 Estimation of subsurface properties

To estimate subsurface parameters from the groundwater response to Earth tides, the analytical solution by Wang et al. (2018) was fitted to the M_2 harmonic component extracted from field data. This analytical describes the well water level fluctuations, $h_{w,o}^{ET}$, caused by the harmonic compression of the subsurface from Earth tides (abbreviated as ET).

The reduction in amplitude of an harmonic signal is described by the ratio between the far field pressure generated by Earth tide strain and the fluid level in the borehole and is known as amplitude ratio (Hsieh et al., 1987)

$$A^{ET} = \frac{h_{w,o}^{ET}}{\epsilon}, \quad (19)$$

where ϵ is the unit-less areal strain. The time lag between the far field pressure and the fluid level in the borehole is known as phase shift Hsieh et al. (1987)

$$\Delta\phi^{ET} = \arg\left(\frac{h_{w,o}^{ET} S_\epsilon}{\epsilon}\right). \quad (20)$$



In theory, the obtained amplitude and phase shift from field measurements (equations 15 and 16) should be the same as those obtained using the analytical solution (Eq. 19 and 20). Since the observed amplitude, A_o^{ET} , and phase shift, $\Delta\phi_o^{ET}$, are measurable in the field, they can be used to fit parameters of the analytical solution of Wang et al. (2018) with a non-linear solver to find roots (Fig. 1g). To do so, the following objective function has to be minimised

$$OF^{ET} = \left| \frac{A_o^{ET} - A^{ET}}{A_o^{ET}} \right| + \left| \frac{\Delta\phi_o^{ET} - \Delta\phi^{ET}}{\Delta\phi_o^{ET}} \right|. \quad (21)$$

Since phase shifts can be orders of magnitude greater than amplitude ratio, OF^{ET} , is normalised to avoid that one term dominates the solution. Assuming that the borehole construction parameters are known (H_a , H_l , r_c and r_w), three parameters can be estimated, i.e., hydraulic conductivity of the aquifer (k_a), vertical hydraulic conductivity of the leaky layer (k_l), and specific storage at constant strain (S_ϵ). Once S_ϵ is obtained, effective porosity can be computed if the material is unconsolidated using (Cheng, 2016; Verruijt, 2013; Wang, 2017)

$$n = \frac{S_\epsilon K_f}{\rho g}, \quad (22)$$

where K_f is the bulk modulus of the fluid ($K_f = 2.2 \cdot 10^9$ Pa for freshwater).

In analogy to Earth tides, the field measurements of barometric pressure and well water levels in the field should match the those obtained by analytical methods. Thus, the obtained amplitude ratio, A_o^{AT} , and phase shift, $\Delta\phi_o^{AT}$, in the field (computed later with Eq. 17 and 18, respectively) can be used to estimate subsurface parameters by iterative non-linear numerical methods (Fig. 1h). The function to minimise is

$$OF^{AT} = \left| \frac{A_o^{AT} - A^{AT}}{A_o^{AT}} \right| + \left| \frac{\Delta\phi_o^{AT} - \Delta\phi^{AT}}{\Delta\phi_o^{AT}} \right|. \quad (23)$$

The non-linear search allows for the iterative fitting of four parameters: hydraulic conductivity of the aquifer (k_a), vertical hydraulic conductivity of the leaky layer (k_l), bulk modulus (K), and specific storage at constant strain (S_ϵ). Additionally, specific storage at constant stress (S_σ) can be estimated using Eq. 11.

Once S_ϵ is estimated, porosity can be computed with Eq. 22. If values of specific storage, S are known (i.e., from a different characterisation method such as pumping tests), then shear modulus can also be estimated as (Cheng, 2016; Verruijt, 2013; Wang, 2017)

$$G = \frac{3}{4} \frac{(1 - K(S - S_\epsilon/\rho g))}{S - S_\epsilon/\rho g}. \quad (24)$$

By effectively combining hydraulic and poroelastic theory, this approach expands the number of parameters that can be estimated.

By solving Eq. 21, aquifer hydraulic conductivity k_a , specific storage at constant strain S_ϵ , and vertical hydraulic conductivity of the aquitard k_l can be estimated. Eq. 23 allows estimation of aquifer hydraulic conductivity k_a , specific storage at constant strain S_σ , vertical hydraulic conductivity of the aquitard k_l , and bulk modulus K . Once specific storage at constant strain is quantified, porosity n , can be estimated with Eq. 22. If the specific storage is known, shear modulus G , can be estimated with equation Eq. 24. Equations 21 and 23 can be solved using non-linear iteration (Fig. 1g and 1h).



The non-linear inversion was performed in two steps to help the iterative method converge to a global minimum instead of a local one. Firstly, the solution space of the objective function was divided into intervals within feasible ranges of subsurface properties, creating a feasible objective space, thus bounding the initial conditions for the least-squares algorithm. Secondly, 1,000 randomly generated values following a log-normal distribution were fed as initial conditions to the least-squares algorithm, the array of parameters that converges to the best fit among them, was considered to be the global minimum of the non-linear search (Aster et al., 2018).

3.4 Hydraulic and geomechanical properties

Values from Earth tide analysis and atmospheric tide analysis are presented in Tables 2 and 3. Further, the estimated aquifer hydraulic conductivity, specific storage at constant strain and aquitard vertical hydraulic conductivity for boreholes B1 and B2 are shown Fig. 5.

Table 2. Estimated subsurface parameters from Earth tide analysis.

Borehole	Non-linear search results			
	k_a [ms^{-1}]	S_ϵ [m^{-1}]	k_l [ms^{-1}]	n [-]
B1	$1.1 \cdot 10^{-5}$	$1.8 \cdot 10^{-6}$	$5.4 \cdot 10^{-8}$	0.37
B2	$1.0 \cdot 10^{-4}$	$3.8 \cdot 10^{-7}$	$1.1 \cdot 10^{-8}$	0.08

Table 3. Estimated subsurface parameters from atmospheric tide analysis.

Borehole	Non-linear search results					
	k_a [ms^{-1}]	S_ϵ [m^{-1}]	k_l [ms^{-1}]	K [GPa]	S_σ [m^{-1}]	n [-]
B1	$1.6 \cdot 10^{-5}$	$1.8 \cdot 10^{-6}$	$8.0 \cdot 10^{-10}$	0.3	$3.5 \cdot 10^{-5}$	0.4
B2	$1.0 \cdot 10^{-4}$	$5.0 \cdot 10^{-7}$	$6.0 \cdot 10^{-8}$	10.0	$1.5 \cdot 10^{-6}$	0.11

The basic assumption of undrained conditions applies to the analytical solutions by Wang et al. (2018) and this study (Eq. 8). To assess whether this condition is fulfilled, both Earth and atmospheric tide analyses, were assessed separately:

1. For Earth tide analysis, Bastias et al. (2022) numerically computed the level of drainage over depth for different arrays of subsurface properties. Despite the estimated k_l being outside the range presented by Bastias et al. (2022), it can be extrapolated. At borehole B1, the aquifer is within undrained conditions. At borehole B2, it is within the transition zone between drained and undrained.



270 2. For atmospheric tide analysis, Wang (2017) defined the depth of undrained conditions as

$$\delta = \sqrt{\frac{2c}{\omega}}, \quad (25)$$

where c is the consolidation coefficient. For boreholes B1 and B2, undrained conditions are found at depths higher than 2.3 and 40.6 m , respectively, under atmospheric tide loading.

Consequently, for the estimated parameters in this study, B2 borders drained conditions, and the generated confined pore pressure by tidal forcing is being diminished. This may influence the estimated properties.

275 The aquifer hydraulic conductivity estimated with PSC complies with previous values of poorly consolidated sands and gravel aquifers in the literature ($5 \cdot 10^{-6} \leq k_a \leq 10^{-3} \text{ m s}^{-1}$) (Freeze and Cherry, 1979; Tickell, 2017) (Fig. 5a, Tables 2 and 3). Note that the estimated value of k_a is lower compared to the pumping tests in the study site (Table B1). Bastias et al. (2022) studied the area of influence of PSC and concluded that PSC is a small-scale characterisation technique where parameters are estimated in the vicinity of the well screen. This might explain the difference between values presented in this study and the ones obtained with pumping tests (Appendix B), as estimates parameters with small-scale methods will tend to give much lower values than obtained from a full-well or packer pumping test, because small-scale analyses may miss the most permeable intervals that make the greatest contribution to the transmissivity (Maliva, 2016). This idea is supported by previous studies that reported several orders of magnitude differences between traditional hydraulic characterisation methods and PSC (Allègre et al., 2016; Zhang et al., 2019; Valois et al., 2022; Qi et al., 2023). The difference was attributed to issues such as the borehole skin effect (Zhang et al., 2019; Valois et al., 2022) and differing model assumptions (Qi et al., 2023). Furthermore, Zhang et al. (2021) showed good agreement between hydraulic parameters of a consolidated subsurface system derived using PSC and laboratory measurements. This supports our observation that PSC results are representative of a smaller sample volume close to the well screen. However, determining the extent of the area around the well screen affected by flow from tidal forces is outside the scope of this work and requires further investigation. Additionally, reconciling the properties derived from both active and passive approaches will require more research.

285 The estimated values of specific storage at constant strain for B1 are within the previously reported values in the literature for sand aquifers, $1.13 \cdot 10^{-6} \leq S_\epsilon \leq 2.27 \cdot 10^{-6} \text{ m}^{-1}$ (Freeze and Cherry, 1979) (Fig. 5b). Porosity, computed with Eq. 22, is also within the reported range, $0.25 \leq n \leq 0.5$ (Freeze and Cherry, 1979). Conversely, borehole B2 shows values of specific storage at constant strain and porosity are below the expected range Tables 2 and 3. There are several potential causes for this, such as the presence of flow paths that create undrained conditions, leading to a reduction in the generated confined pore pressure and exposing the limitations of passive methods for this borehole. Furthermore, the degree of aquifer consolidation is limited, and the length of the well screen is not representative of the full depth of the aquifer. These factors were not explored in this study and should be the focus of future numerical investigations to better understand their effects on the results.

300 The estimated aquifer bulk modulus values (Table 3) were consistent with literature values for sands and gravels, typically between $5 \cdot 10^{-2} \text{ GPa}$ and $3 \cdot 10^1 \text{ GPa}$ (Das and Das, 2008; Look, 2007). If it is assumed that the average variability of the hydraulic properties in the aquifer is low (Fig. B1b), the values presented in Table B1 (wells W7, W8, W9 and W10) can be used to estimate shear modulus using Eq. 24. Estimated shear modulus values were 0.7 and 0.03 GPa for B1 and B2

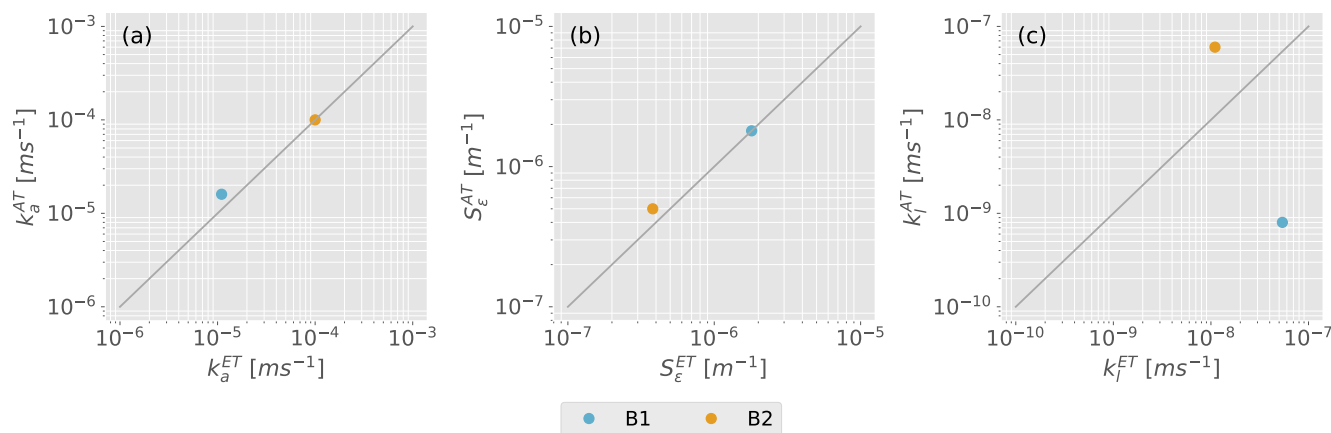


Figure 5. Comparison of the subsurface parameters estimated independently using the well water level response to Earth tides and atmospheric tides: (a) hydraulic conductivity of the aquifer, (b) specific storage at constant strain, (c) vertical hydraulic conductivity of the aquitard.

respectively. We note that these values are consistent with expectations reported in the literature for similar lithological settings, e.g., typically between $8 \cdot 10^{-3} \text{ GPa}$ and $9 \cdot 10^3 \text{ GPa}$ (Das and Das, 2008; Look, 2007).

Compared to the previous analytical solution presented by Rojstaczer and Riley (1990), which describes flow to wells due to barometric loading, the derived analytical solution in this study simplifies the pore pressure wave generated in the vadose zone by assuming that only small vertical flow occurs in the confined layer. Moreover, the solution of Rojstaczer and Riley (1990) requires knowledge of vadose zone properties that are difficult to determine. Furthermore, the continuity equation is solved in terms of the mean stress equation, allowing for the estimation of mechanical parameters such as bulk modulus and specific storage at constant stress. As shown in our work, this extends the current range of parameters that can be estimated passively (McMillan et al., 2019).

While we present a new analytical solution, we are unable to compare or validate geomechanical results due to a lack of independent measurements. Additionally, the literature comparing subsurface properties using PSC from different methods is sparse and contains somewhat conflicting conclusions (Allègre et al., 2016; Zhang et al., 2019; Valois et al., 2022; Qi et al., 2023; Zhang et al., 2021). This is likely due to the fact that subsurface investigations often focus on determining hydraulic properties such as hydraulic conductivity and specific storage, which are critical for understanding subsurface fluid flow. Obtaining geomechanical information such as bulk modulus, shear modulus, and stress state can be challenging and may require additional investigation techniques. However, Rau et al. (2022) noted that in-situ stress conditions, stress anisotropy and scale differences complicate comparisons with laboratory methods. We believe that systematic investigations in different archetypes of formations, including the use of borehole geophysical investigation techniques and careful laboratory testing of material samples, could help to clarify scale and heterogeneity influences, reconcile the different theories, and provide further confidence in values derived from PSC.



4 Conclusions

325 We have introduced a novel analytical solution based on the mean stress flow equation for modelling flow to wells induced
by atmospheric loading. We integrate this mean stress solution into a comprehensive workflow for estimating subsurface
hydraulic and geomechanical properties using the groundwater response to Earth and atmospheric tides, applied this to a
standard groundwater monitoring data set from the Northern Territory (Australia) and discussed the results with hydraulic
properties from pumping tests and geomechanical literature values for similar lithological settings. Our new solution allows
330 estimation of hydraulic conductivity of the aquifer, vertical hydraulic conductivity of the aquitard, porosity, specific storage at
constant strain, specific storage at constant stress and bulk modulus. The advantages are estimation of additional subsurface
properties without the need for knowledge of vadose zone properties.

We compared the hydraulic properties estimated independently using the groundwater response to Earth tides and atmo-
spheric pressure. The estimated values of aquifer hydraulic conductivity with Earth tidal analysis were $1.1 \cdot 10^{-5} \text{ m s}^{-1}$ and
335 $1.1 \cdot 10^{-4} \text{ m s}^{-1}$ for borehole B1 and B2, respectively. Meanwhile, with the mean stress solution, the estimated values of aquifer
hydraulic conductivity were $1.6 \cdot 10^{-5} \text{ m s}^{-1}$ and $1.0 \cdot 10^{-4} \text{ m s}^{-1}$ for borehole B1 and B2, respectively. These estimated values
were lower than those estimated using pumping tests for the region between Mary River National Park and Kakadu National
Park (ranging from $6 \cdot 10^{-4}$ to $8 \cdot 10^{-5} \text{ m s}^{-1}$). This difference is consistent with the literature and supports the idea that PSC
is a small-scale characterisation method.

340 The estimated specific storage at constant strain for borehole B2 was $3.8 \cdot 10^{-7}$ and $5.0 \cdot 10^{-7} \text{ m}^{-1}$ with Earth tidal analysis
and the mean stress equation, respectively. This indicates that the response near borehole B2 is drained since the estimated
values are lower than the reported bounds in the literature. Consequently, the drained conditions reduce the confined pore
pressure generated by tides. The estimated values of aquitard vertical hydraulic conductivity differed from the pumping tests
by orders of magnitude but suggest that the aquifer in both boreholes is semi-confined with small leakage.

345 The bulk and shear moduli aligned with literature values for the formation type, confirming that PSC has the potential to
enhance field investigations. However, for PSC to be applied successfully, it is necessary for the basic physical assumptions
underlying the analytical solutions to be valid. This can be challenging to determine in situations such as confined and undrained
hydraulic conditions or an unconsolidated system where the Biot coefficient is unknown. As a result, PSC can only be applied
in hydrogeological settings that adhere to the theoretical framework.

350 Compared to established methods like hydraulic testing, using PSC requires a better understanding of hydraulic and hydro-
geomechanical theory as well as signal processing. However, PSC is less costly and effort-intensive because it only requires
monitoring datasets that typically meet standard practice criteria. The literature reflects confusion about the suitability of theory
and a lack of geomechanical testing alongside hydraulic testing, making it challenging to validate poroelastic properties. Sys-
tematic investigations involving a range of archetypal formations with a combination of hydraulic, geophysical, geotechnical
355 field and laboratory tests are needed to validate PSC. This would help compare properties from rigid and elastic formations,
reconcile theories, and support groundwater and geotechnical investigations.



Code availability. Python based code which streamlines the data analysis and subsurface properties estimation are provided after submission.

Data availability. The datasets are provided to editors and reviewers during the review process and to the public should this work be accepted.

Code and data availability. The code is provided to editors and reviewers during the review process and to the public should this work be accepted.
360

Appendix A

The hydraulic head measurements in borehole B1 and B2 are shown in Fig. A1. Outliers were detected and eliminated with the procedure described in Section 3.2.

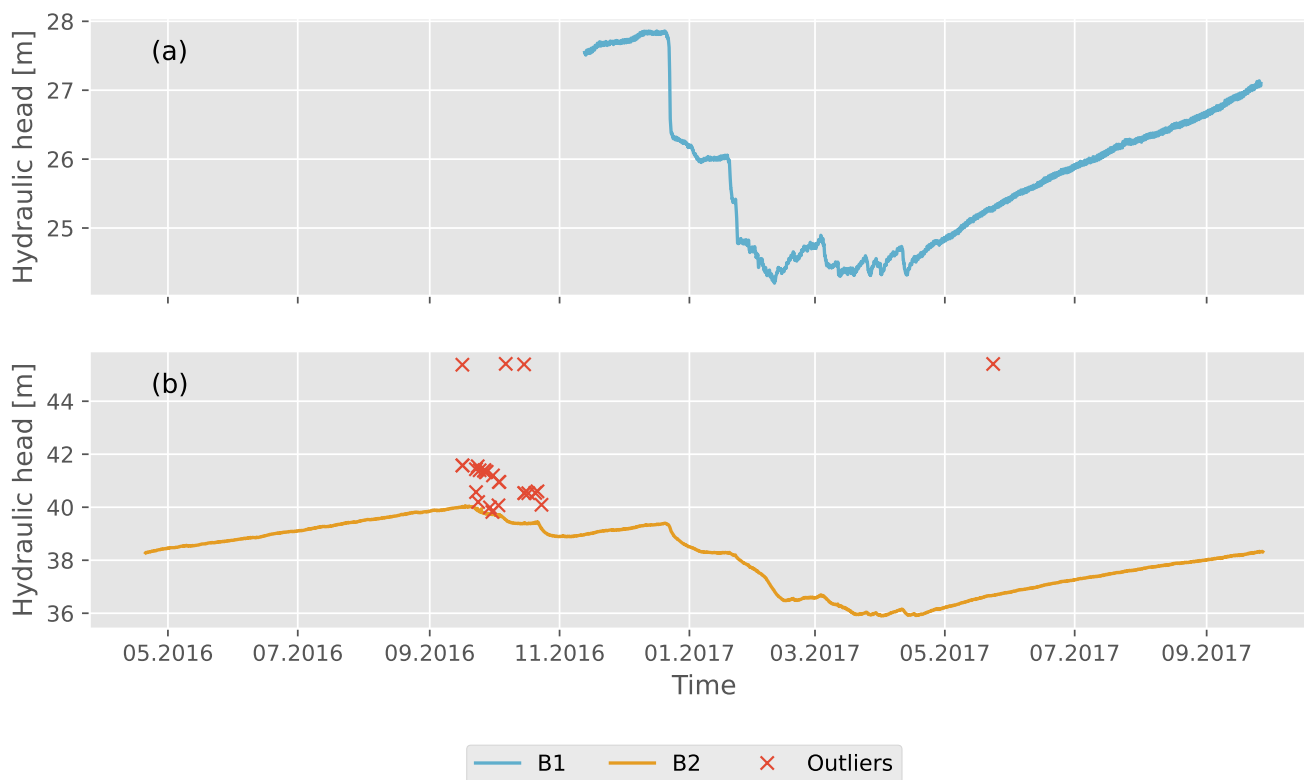


Figure A1. Hydraulic head time series and outliers measured in boreholes (a) B1 and (b) B2.



365 Computed areal Earth tide strain, measured barometric pressure and hydraulic head of borehole B1 and B2 were de-trended using a moving median filter with 3-day window, Sec. 3.2 and Fig. A2.

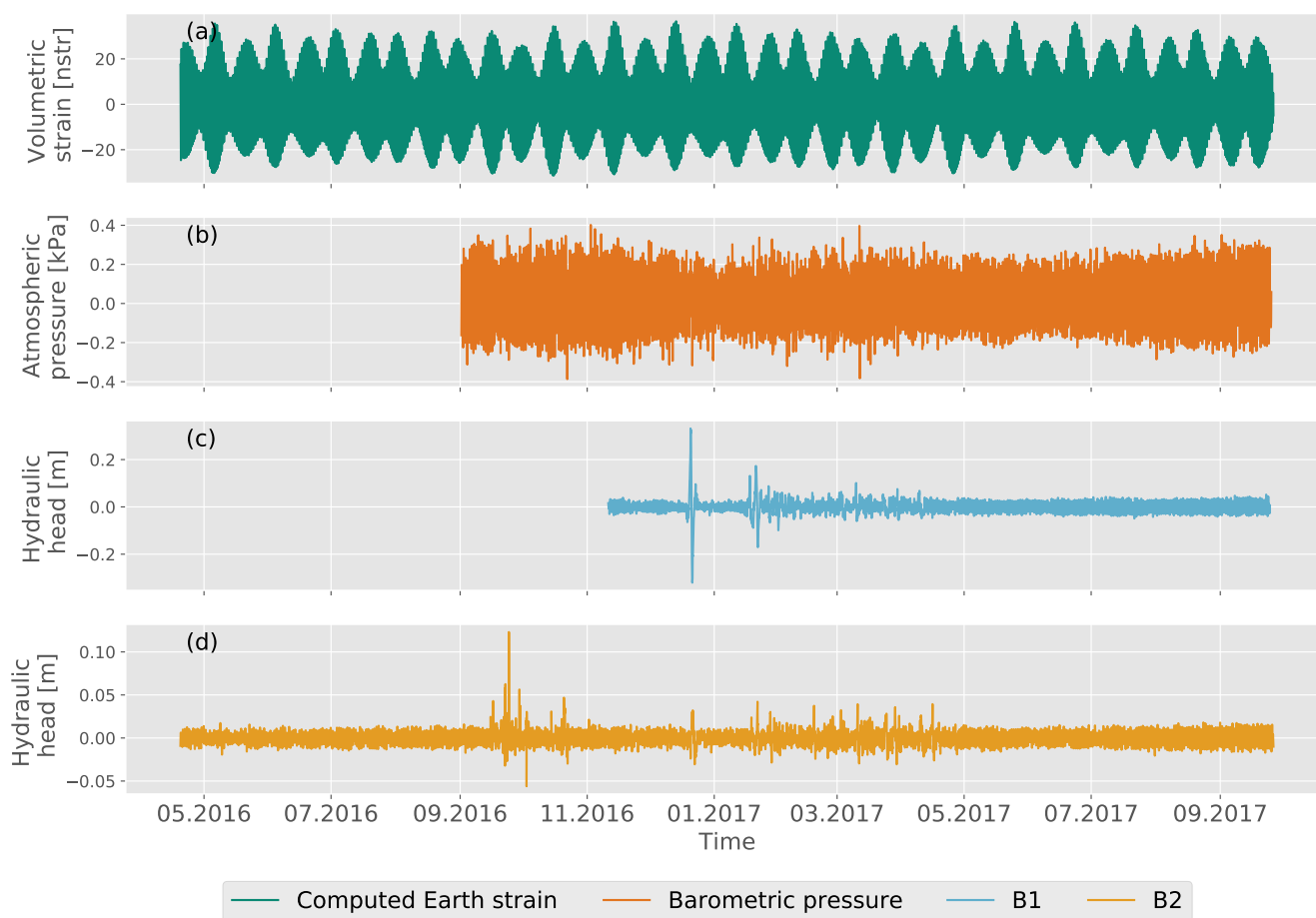


Figure A2. The corresponding de-trended time series showing only components with frequencies up to 3 cpd; (a) computed Earth strain, (b) measured atmospheric pressure, hydraulic head (c) B1 and (d) B2.

Harmonic constituents were obtained applying harmonic least squares (HALS), results of amplitude and phase shift to the M_2 signal are shown in Table A1. Analogously, the amplitude and phase shift to the S_2 signal are shown in Table A2.

Table A1. Amplitude ratio and phase shift obtained with HALS for the M_2 constituent.

Borehole	A^{ETP} [-]	$\Delta\phi^{ETP}$ [°]	A^{GW} [m]	$\Delta\phi^{GW}$ [°]	A_o^{ET} [m]	$\Delta\phi_o^{ET}$ [°]
B1	$26.57 \cdot 10^{-9}$	0.52	0.0015	-0.061	57386.49	0.59
B2	$26.65 \cdot 10^{-9}$	1.74	0.0012	1.76	46710.38	-0.02



Table A2. Amplitude ratio and phase shift obtained with HALS for the S_2 constituent.

Borehole	A^{ATP} [kPa]	$\Delta\phi^{ATP}$ [°]	A^{GW} [m]	$\Delta\phi^{GW}$ [°]	A_o^{AT} [-]	$\Delta\phi_o^{AT}$ [°]
B1	0.12	2.84	$1.0 \cdot 10^{-2}$	2.83	0.82	-0.71
B2	0.12	-0.33	$0.58 \cdot 10^{-3}$	-0.20	0.47	7.83



Appendix B

Time–drawdown data from five two-well pumping tests in the Mary–Wildman rivers area were reinterpreted using appropriate drawdown solutions using a two-step process (see Table B1 and W1 to W10 in Figure B1a) (Turnadge et al., 2018). The time–drawdown data, were used to identify appropriate pumping test analysis solutions. These included: the solutions of Barker (1988) for fractured rock flow under confined conditions; Hantush (1960) for leaky conditions; and Neuman (1974) for unconfined conditions.

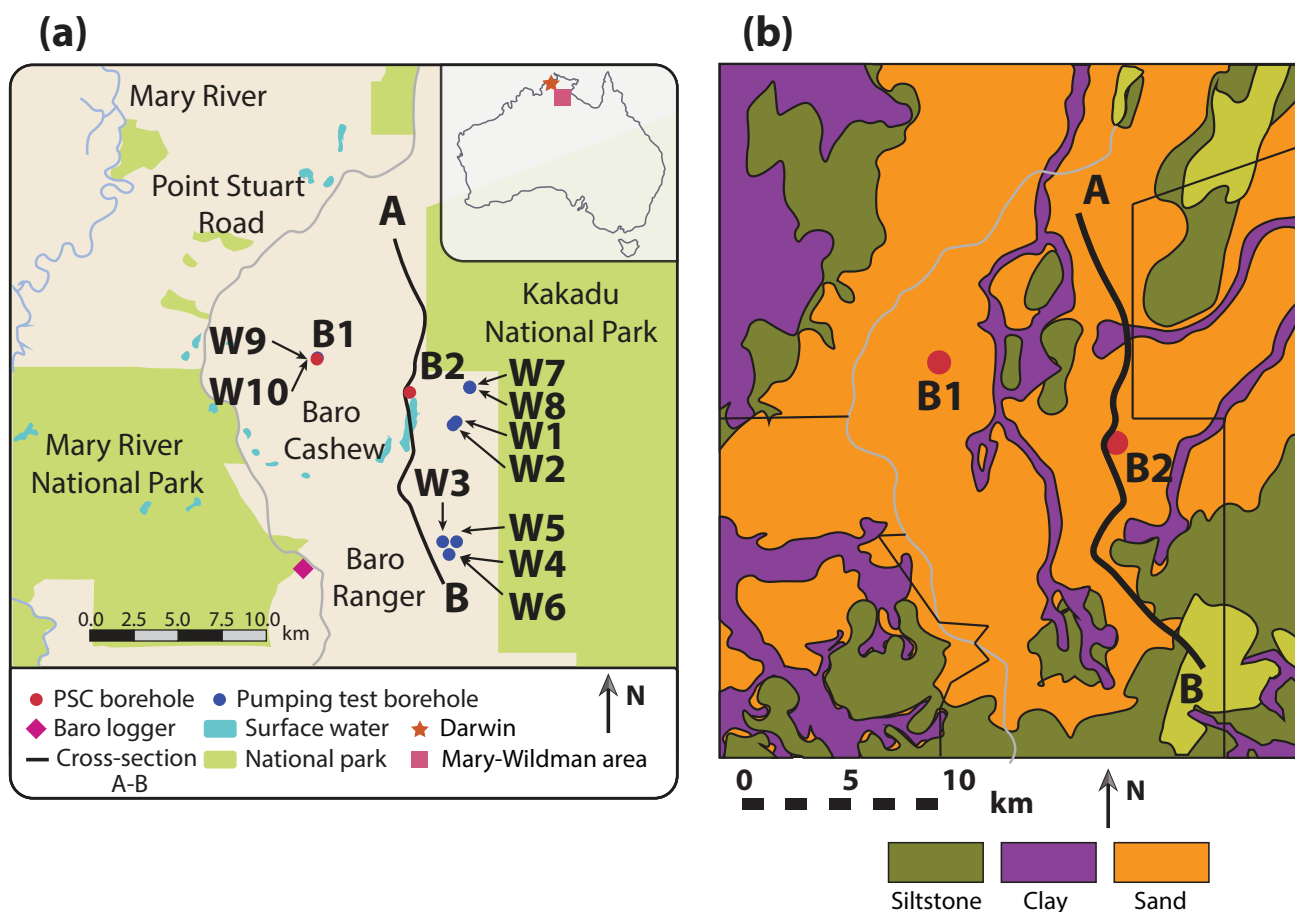


Figure B1. Map of the study site. (a) shows PSC boreholes, barometric sensor and location of the wells where pumping tests were performed (wells W1 to W10). (b) shows the surface geology of the Mesozoic/Cenozoic strata (modified from NT Geological Survey digital data, (Tickell, 2017))



Table B1. Details of five historical two-well pumping tests undertaken in the Mary–Wildman rivers area, including aquifer types interpreted from time–drawdown responses and forward solutions used to estimate aquifer hydraulic properties via model inversion. Hydraulic property values are displayed with root mean square error of optimised least squares solution. For each estimated parameter, the optimal value derived from least squares estimation is provided, as well as the approximate 95 % confidence interval.

Production well ID	Observation well ID	Attributed aquifer	Confinement type	Inversion solution	RMSE [m]	$k_a \cdot 10^{-4}$ [$m s^{-1}$]	$S_s \cdot 10^{-5}$ [m^{-1}]	$S_y \cdot 10^{-3}$ [-]		
W1	-	W2	-	Cretaceous sand	Unconfined	Neuman (1974)	$1 \cdot 10^{-2}$	4.1 ± 0.3	N/A	1.0 ± 0.4
RN023158		RN023230								
W3	-	W4	-	Wildman Siltstone	Confined	Barker (1988)	$9 \cdot 10^{-4}$	4.6 ± 0.9	8.0 ± 0.6	N/A
RN024668		RN024596								
W5	-	W6	-	Wildman Siltstone	Confined	Barker (1988)	$2 \cdot 10^{-3}$	0.8 ± 0.2	1.0 ± 0.8	N/A
RN024669		RN024228								
W7	-	W8	-	Cretaceous sand	Leaky	Hantush (1960)	$1 \cdot 10^{-4}$	6.3 ± 0.3	5.0 ± 0.5	N/A
RN024763		RN024764								
W9	-	W10	-	Cretaceous sand	Leaky	Hantush (1960)	$1 \cdot 10^{-3}$	4.1 ± 0.4	7.0 ± 0.8	N/A
RN039769		RN039768								



375 *Author contributions.* JMBE analysed the datasets, created the figures and wrote the first manuscript draft. CT and RC provided the datasets and reviewed the work. CT analysed the pumping tests. PB reviewed the manuscript and provided conceptual suggestions. GCR obtained the funding, supervised JMBE and actively contributed to all aspects of this work.

Competing interests. The authors declare that they have no competing interests.

380 *Acknowledgements.* This project has received funding from the German Research Council (DFG) grant agreement number 424795466. The authors would like to thank the following individuals who conducted field work to collect datasets used here: Steven Tickell, Ursula Zaar, Gary Willis, Steve Dwyer, Emma Jackson, Ian Bate, Stanley Smith, Alec Deslandes, Karen Barry, Simone Gelsinari, and Julia Knollmann.



References

- Acworth, R. I., Halloran, L. J., Rau, G. C., Cuthbert, M. O., and Bernardi, T. L.: An objective frequency domain method for quantifying confined aquifer compressible storage using Earth and atmospheric tides, *Geophysical Research Letters*, 43, 11–671, 2016.
- Acworth, R. I., Rau, G. C., Halloran, L. J., and Timms, W. A.: Vertical groundwater storage properties and changes in confinement determined using hydraulic head response to atmospheric tides, *Water Resources Research*, 53, 2983–2997, 2017.
- 385 Allègre, V., Brodsky, E. E., Xue, L., Nale, S. M., Parker, B. L., and Cherry, J. A.: Using earth-tide induced water pressure changes to measure in situ permeability: A comparison with long-term pumping tests, *Water Resources Research*, 52, 3113–3126, <https://doi.org/10.1002/2015WR017346>, 2016.
- Arditty, P. C., Ramey, H. J., and Nur, A. M.: Response of a closed well-reservoir system to stress induced by earth tides, in: *Spe annual fall technical conference and exhibition*, OnePetro, 1978.
- 390 Aster, R. C., Borchers, B., and Thurber, C. H.: *Parameter estimation and inverse problems*, Elsevier, 2018.
- Barker, J.: A generalized radial flow model for hydraulic tests in fractured rock, *Water Resources Research*, 24, 1796–1804, 1988.
- Bastias, J., Rau, G. C., and Blum, P.: Groundwater responses to Earth tides: Evaluation of analytical solutions using numerical simulation, *Journal of Geophysical Research: Solid Earth*, 127, <https://doi.org/10.1029/2022JB024771>, 2022.
- 395 Biot, M. A.: General theory of three-dimensional consolidation, *Journal of applied physics*, 12, 155–164, 1941.
- Bodvarsson, G.: Confined fluids as strain meters, *Journal of Geophysical Research*, 75, 2711–2718, 1970.
- Bredehoeft, J. D.: Response of well-aquifer systems to Earth tides, *Journal of Geophysical Research*, 72, 3075–3087, 1967.
- Cheng, A. H.-D.: *Poroelasticity*, vol. 27, Springer, 2016.
- Cooper Jr, H. H., Bredehoeft, J. D., Papadopoulos, I. S., and Bennett, R. R.: The response of well-aquifer systems to seismic waves, *Journal of Geophysical Research*, 70, 3915–3926, 1965.
- 400 Cutillo, P. A. and Bredehoeft, J. D.: Estimating aquifer properties from the water level response to earth tides, *Groundwater*, 49, 600–610, 2011.
- Das, B. M. and Das, B.: *Advanced soil mechanics*, vol. 270, Taylor & Francis New York, 2008.
- Doan, M.-L., Brodsky, E. E., Prioul, R., and Signer, C.: Tidal analysis of borehole pressure-A tutorial, University of California, Santa Cruz, 25, 27, 2006.
- 405 Domenico, P. A. and Schwartz, F. W.: *Physical and chemical hydrogeology*, John Wiley & Sons, 1997.
- Freeze, R. A. and Cherry, J. A.: *Groundwater*, Prentice Hall, Inc., Upper Saddle River, NJ 07458, <http://hydrogeologistswithoutborders.org/wordpress/1979-toc/>, 1979.
- Gao, X., Sato, K., and Horne, R. N.: General solution for tidal behavior in confined and semiconfined aquifers considering skin and wellbore storage effects, *Water Resources Research*, 56, e2020WR027195, 2020.
- 410 Guo, H., Brodsky, E., Goebel, T., and Cladouhos, T.: Measuring Fault Zone and Host Rock Hydraulic Properties Using Tidal Responses, *Geophysical Research Letters*, 48, e2021GL093986, 2021.
- Hantush, M. S.: Modification of the theory of leaky aquifers, *Journal of Geophysical Research*, 65, 3713–3725, 1960.
- Hsieh, P. A., Bredehoeft, J. D., and Farr, J. M.: Determination of aquifer transmissivity from Earth tide analysis, *Water resources research*, 23, 1824–1832, 1987.
- 415 Lai, G., Ge, H., and Wang, W.: Transfer functions of the well-aquifer systems response to atmospheric loading and Earth tide from low to high-frequency band, *Journal of Geophysical Research: Solid Earth*, 118, 1904–1924, 2013.



- Lai, G., Ge, H., Xue, L., Brodsky, E. E., Huang, F., and Wang, W.: Tidal response variation and recovery following the Wenchuan earthquake from water level data of multiple wells in the nearfield, *Tectonophysics*, 619, 115–122, 2014.
- 420 Le Borgne, T., Bour, O., De Dreuzy, J., Davy, P., and Touchard, F.: Equivalent mean flow models for fractured aquifers: Insights from a pumping tests scaling interpretation, *Water Resources Research*, 40, 2004.
- Liang, X., Wang, C.-Y., Ma, E., and Zhang, Y.-K.: Effects of Unsaturated Flow on Hydraulic Head Response to Earth Tides—An Analytical Model, *Water Resources Research*, 58, e2021WR030337, 2022.
- Look, B. G.: *Handbook of geotechnical investigation and design tables*, Taylor & Francis, 2007.
- 425 Maliva, R. G.: *Aquifer characterization techniques*, vol. 10, Springer, 2016.
- McMillan, T. C., Rau, G. C., Timms, W. A., and Andersen, M. S.: Utilizing the impact of Earth and atmospheric tides on groundwater systems: A review reveals the future potential, *Reviews of Geophysics*, 57, 281–315, 2019.
- Meinzer, O. E.: *Ground water in the United States, a summary of ground-water conditions and resources, utilization of water from wells and springs, methods of scientific investigation, and literature relating to the subject*, Tech. rep., U.S. G.P.O., <http://pubs.er.usgs.gov/publication/wsp836D>, 1939.
- 430 Merritt, M. L.: *Estimating hydraulic properties of the Floridan aquifer system by analysis of earth-tide, ocean-tide, and barometric effects, Collier and Hendry Counties, Florida*, 3, US Department of the Interior, US Geological Survey, 2004.
- Neuman, S. P.: Effect of partial penetration on flow in unconfined aquifers considering delayed gravity response, *Water resources research*, 10, 303–312, 1974.
- 435 Pham-Gia, T. and Hung, T. L.: The mean and median absolute deviations, *Mathematical and Computer Modelling*, 34, 921–936, 2001.
- Qi, Z., Shi, Z., and Rasmussen, T. C.: Time- and frequency-domain determination of aquifer hydraulic properties using water-level responses to natural perturbations: A case study of the Rongchang Well, Chongqing, southwestern China, *Journal of Hydrology*, 617, 128820, <https://doi.org/https://doi.org/10.1016/j.jhydrol.2022.128820>, 2023.
- Rahi, K. A. and Halihan, T.: Identifying aquifer type in fractured rock aquifers using harmonic analysis, *Groundwater*, 51, 76–82, 2013.
- 440 Rau, G.: *PyGTide: A Python module and wrapper for ETERNA PREDICT to compute synthetic model tides on Earth*, Zenodo [code], 2018.
- Rau, G. C., Cuthbert, M. O., Acworth, R. I., and Blum, P.: Technical note: Disentangling the groundwater response to Earth and atmospheric tides to improve subsurface characterisation, *Hydrology and Earth System Sciences*, 24, 6033–6046, <https://doi.org/10.5194/hess-24-6033-2020>, 2020.
- Rau, G. C., McMillan, T. C., Andersen, M. S., and Timms, W. A.: In situ estimation of subsurface hydro-geomechanical properties using the groundwater response to semi-diurnal Earth and atmospheric tides, *Hydrology and Earth System Sciences*, 26, 4301–4321, 2022.
- 445 Robinson, E. S. and Bell, R. T.: Tides in confined well-aquifer systems, *Journal of Geophysical Research*, 76, 1857–1869, 1971.
- Roeloffs, E. A., Burford, S. S., Riley, F. S., and Records, A. W.: Hydrologic effects on water level changes associated with episodic fault creep near Parkfield, California, *Journal of Geophysical Research*, 94, 12387, <https://doi.org/10.1029/jb094ib09p12387>, 1989.
- Rojstaczer, S.: Determination of fluid flow properties from the response of water levels in wells to atmospheric loading, *Water Resources Research*, 24, 1927–1938, 1988.
- 450 Rojstaczer, S. and Riley, F. S.: Response of the water level in a well to earth tides and atmospheric loading under unconfined conditions, *Water Resources Research*, 26, 1803–1817, 1990.
- Schweizer, D., Ried, V., Rau, G. C., Tuck, J. E., and Stoica, P.: Comparing Methods and Defining Practical Requirements for Extracting Harmonic Tidal Components from Groundwater Level Measurements, *Mathematical Geosciences*, <https://doi.org/10.1007/s11004-020-09915-9>, 2021.
- 455

Shi, Z. and Wang, G.: Aquifers switched from confined to semiconfined by earthquakes, *Geophysical Research Letters*, 43, 11–166, 2016.

Tickell, Z.: Water Resources of the Wildman River Area. Northern Territory Government, <https://territorystories.nt.gov.au/10070/428586/0/53>, 2017.

460 Turnadge, C., Crosbie, R., Tickell, S., Zaar, U., Smith, S., Dawes, W., Davies, P., Harrington, G., and Taylor, A.: Hydrogeological characterisation of the Mary–Wildman rivers area, Northern Territory, 2018.

Valois, R., Rau, G. C., Vouillamoz, J.-M., and Derode, B.: Estimating hydraulic properties of the shallow subsurface using the groundwater response to Earth and atmospheric tides: a comparison with pumping tests, *Water Resources Research*, 58, e2021WR031666, 2022.

Van der Kamp, G. and Gale, J.: Theory of earth tide and barometric effects in porous formations with compressible grains, *Water Resources Research*, 19, 538–544, 1983.

465 Verruijt, A.: Theory and problems of poroelasticity, Delft University of Technology, 71, 2013.

Wang: Theory of linear poroelasticity with applications to geomechanics and hydrogeology, Princeton University Press, 2017.

Wang, C. Y., Doan, M. L., Xue, L., and Barbour, A. J.: Tidal response of groundwater in a leaky aquifer—Application to Oklahoma, *Water Resources Research*, 54, 8019–8033, 2018.

470 Wenzel, H.-G.: The nanoGal software: Earth tide data processing package: Eterna 3.3, *Bulletin d’Informations des Marées Terrestres*, 124, 9425–9439, 1996.

Xue, L., Brodsky, E. E., Erskine, J., Fulton, P. M., and Carter, R.: A permeability and compliance contrast measured hydrogeologically on the San Andreas Fault, *Geochemistry, Geophysics, Geosystems*, 17, 858–871, 2016.

Zhang, S., Shi, Z., and Wang, G.: Comparison of aquifer parameters inferred from water level changes induced by slug test, earth tide and earthquake – A case study in the three Gorges area, *Journal of Hydrology*, 579, 124–169, 475 <https://doi.org/https://doi.org/10.1016/j.jhydrol.2019.124169>, 2019.

Zhang, Y., Wang, C. Y., Fu, L. Y., and Yang, Q. Y.: Are Deep Aquifers Really Confined? Insights From Deep Groundwater Tidal Responses in the North China Platform, *Water Resources Research*, 57, e2021WR030195, 2021.